Available online at www.sciencedirect.com
ScienceDirect
Deep-Sea Research I 53 (2006) 1439–1459
DEEP-SEA RESEARCH PART I
www.elsevier.com/locate/dsr

# Bio-optical properties of high chlorophyll Case 1 waters and of yellow-substance-dominated Case 2 waters

André Morel*, Bernard Gentili, Malik Chami, Joséphine Ras

*Laboratoire d'Océanographie de Villefranche, CNRS/UPMC, 06238 Villefranche-sur-mer CEDEX, France*

Received 22 November 2005; received in revised form 19 July 2006; accepted 20 July 2006

**Abstract**

Case 1 waters with high chlorophyll content can be encountered as soon as the nutrient availability is high enough and the terrestrial influence by land drainage is negligible. Offshore oceanic blooms and upwelling zones along arid coasts are instances of such waters. Their bio-optical properties are less documented compared to those of mesotrophic or oligotrophic waters. A coherent set of measurements of bio-geochemical properties (algal pigments, suspended particulate matter), inherent optical properties (absorption and scattering by water bodies and by particulate material), and apparent optical properties (hyperspectral reflectance and diffuse attenuation coefficients) was obtained within the Benguela Current, i.e. in an upwelling area with arid climate and no runoff. These data allow the bio-optical relationships in eutrophic Case 1 waters to be analyzed, and their natural variability to be compared with that previously observed in less productive waters. In addition, a comparison between eutrophic Case 1 waters and yellow substance dominated Case 2 waters can be made, since such waters are also present in the area under investigation. The coherence between the inherent and apparent optical properties is also analyzed via inversion. Despite some deficiencies in their parameterization, the existing bio-optical models for Case 1 waters were proven to be valid such that they can be extended without significant discontinuities toward the domain of high concentration (up to $30\,mg\,m^{-3}$). In particular, those models in use for the interpretation of remotely sensed ocean color continue to apply, even if the sensitivity of current algorithms for the chlorophyll retrieval weakens owing to inescapable physical limitations in the case of high concentrations.


*Keywords:* Optical oceanography; Bio-optics; Case-1 waters; High chlorophyll; Yellow substance

## 1. Introduction and motivation

High chlorophyll concentrations are most often encountered in optically complex coastal (Case 2) waters. Offshore vernal blooms, or upwelling areas along arid coasts with steep slopes, and no runoff, are typical examples of high-chlorophyll Case 1 waters, whose bio-optical properties are less documented than those with low or moderate chlorophyll content. Oligotrophic and mesotrophic waters occupy much wider zones than eutrophic ones, and partly for this reason, the former have been more studied (in contrast, during the International Decade of Ocean Exploration, 1970–1980, emphasis was put on upwelling areas and eastern boundary currents, but at that time optical

*Corresponding author. Tel.: +33 4 9376 37 11; fax: +33 4 93763739.
*E-mail address:* morel@obs-vlfr.fr (A. Morel).

0967-0637/$ - see front matter © 2006 Published by Elsevier Ltd.
doi:10.1016/j.dsr.2006.07.007

measurements were not systematic). To illustrate the scarcity of observations, it can be noted that in the SeaBAM dataset (SeaWiFS Bio-optical Algorithm Mini-workshop; O'Reilly et al., 1998) less than 3% of observations were made in waters with chlorophyll concentration, hereafter denoted (Chl), above $3\,mg\,m^{-3}$. In the recent NASA bio-Optical Marine Algorithm Dataset (NOMAD, Werdell and Bailey, 2005), 8% of the observations are for $(Chl) > 5\,mg\,m^{-3}$ (HPLC-determined). Similarly, in the dataset used by Morel and Maritorena (2001), 23 (Chl) values (over 255) exceeded $5\,mg\,m^{-3}$.

Significant relationships between the optical properties and (Chl) can be empirically derived in Case 1 waters. With less data in eutrophic waters, these relationships are presently less ascertained, and apparently more noisy (O'Reilly et al., 1998). Besides, there would be some reasons to expect more variability in these relationships at high (Chl). Indeed, when a bloom occurs, often an opportunistic algal species dominates; such prevailing species may differ from one blooming situation to another one, and thus generate differences in optical properties. In addition, if the Case 1 water optical properties are regulated primarily by the algal abundance, they equally depend on the relative proportions of living algae and accompanying organisms (heterotrophs) and generated detrital material (particulate and dissolved). According to the age of the oceanic bloom or, in upwelling zones, according to the residence time of the drifting upwelled waters within the well-lit zone, these relative proportions likely change with time, and in this way may modify the relationships between the bulk optical properties and (Chl), used as a single index.

During a recent cruise in the Benguela upwelling system, a considerable number of bio-optical observations were made in waters where phytoplankton were actively growing. This dataset allows the variability in the bio-optical properties in such high-Chl waters to be analyzed, and it provides the possibility of examining the applicability of existing bio-optical models in this (Chl) range.

## 2. The "Bencal" cruise

The scientific objectives and activities of the Benguela Calibration (BENCAL) cruise on board the South African Fisheries Research Ship *Africana* (4–18 October 2002) have been described in a detailed report (Barlow et al., 2003). A rather complete set of hyperspectral measurements of both inherent and apparent optical properties was obtained. These observations were made in particular (but not exclusively) in support of calibration and validation of ocean color satellite observations (SeaWiFS, MERIS and MODIS). The area selected for this cruise (see map in Fig. 1) was the southern Benguela which is known for high phytoplankton concentration triggered by an active coastal upwelling. Most of the stations were located inside this zone. The total chlorophyll *a* concentration ranged between 1 and $29\,mg\,m^{-3}$ (average value 8.0). In addition and for comparison, a few other stations (see map) were located offshore (~400 km) to reach "blue" mesotrophic waters, where (Chl) was between 0.25 and $0.5\,mg\,m^{-3}$ (see Table 1). If the number of stations remains limited in a statistical sense, the panoply of techniques used and the simultaneity of the measurements allow a thorough analysis of a eutrophic regime to be carried out.

The western South African coast is arid, so that the contribution of runoff to the coastal waters is minimal. Therefore, turbid Case-2 waters are a priori not expected in this zone. Nevertheless, under the effect of waves, re-suspension of locally formed sediments, or mobilization of organic compounds from the bottom and sea grass, cannot be excluded, at least in the shallowest waters. It is thus necessary to closely examine the status of each station within the scheme of a Case1/Case 2 classification. For that, several criteria can be used, as explained below after the methods and available data are presented.

## 3. Methods and data

The full set of determinations carried out during BENCAL is described in detail in the report mentioned above. Only the measurements of direct use in the present study are briefly described in what follows.

The LI-1800 UW spectroradiometer (LI-COR instruments) which is equipped with a flat cosine collector was used to determine spectrally (from 305 to 800 nm), and at discrete depths ($z$), the planar irradiance (expressed as $W\,m^{-2}\,nm^{-1}$). Downward and upward spectral irradiances, $E_d(\lambda, z)$ and $E_u(\lambda, z)$ respectively, were measured during two separate casts, effected in rapid succession. The data, recorded every 2 nm, were corrected for changing irradiance, determined with a PAR sensor that monitored the solar radiation incident upon the deck. Slight shifts in solar radiation during the

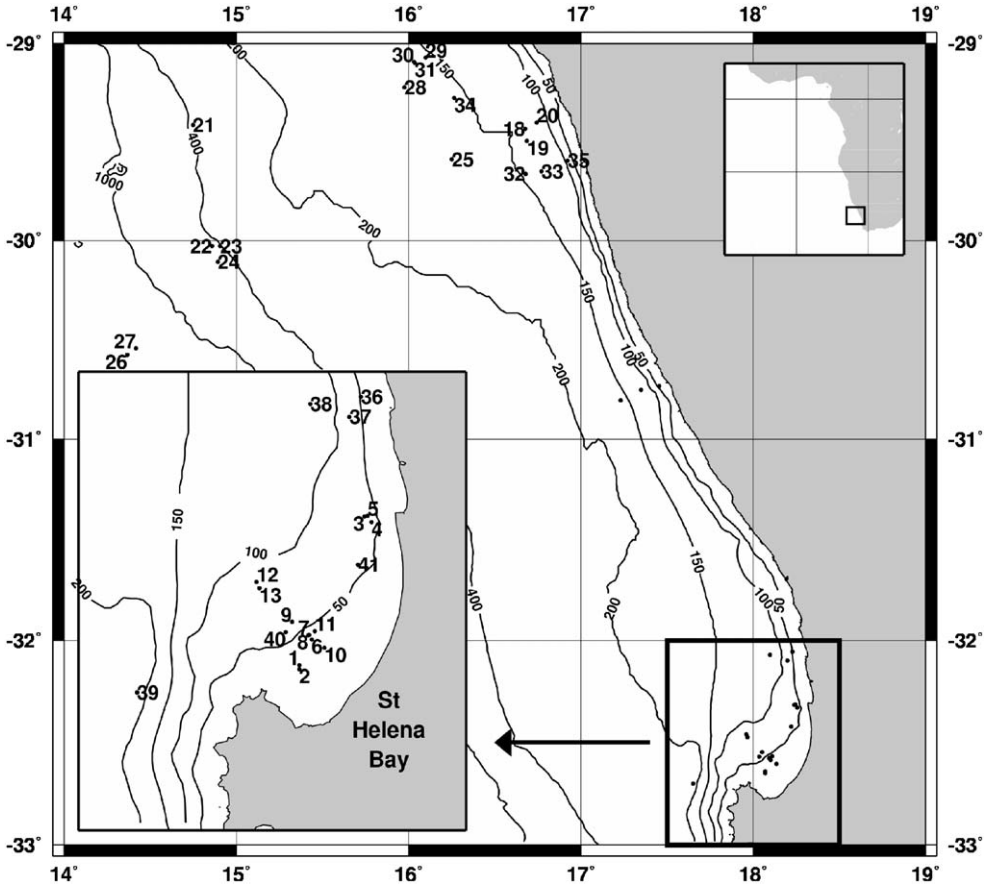


Fig. 1. Location of the Bencal stations and bathymetry (source Smith-Sandwell/GEBCO grid). The northernmost stations (#28–31) are located about 50 km south of the turbid Orange River mouth.

experiments could be easily corrected for, and the $E_d(\lambda, z)$ and $E_u(\lambda, z)$ were all normalized to the same incident irradiance above the surface. In case of important changes (varying cloudiness) the correction is questionable, and such noisy measurements were discarded. Fortunately, the sky conditions were generally excellent (see Table 2 in Barlow et al., 2003). A calibrated pressure sensor allowed the depth of measurement to be accurately determined (within 10 cm). However, near-surface upward irradiance measurements, $E_u(\lambda, \varepsilon)$, were performed at shallow depths ($\varepsilon$) compatible with ship's roll and the presence of waves and swell; this depth ($\varepsilon$ from 0.5 to 2.5 m, approximately) was thus varying during the spectral measurement (lasting about 30 s) and cannot be accurately known, notwithstanding the accuracy of the gauge.

The diffuse attenuation coefficients, $K_d(\lambda)$, were computed for the upper layer as

$$K_d(\lambda) = (1/z)\ln[E_d(\lambda, 0^-)/E_d(\lambda, z)].$$

$E_d(\lambda, 0^-)$ just below the surface is derived from $E_d(\lambda, 0+)$ measured above the surface after correction for the transmission through the interface (transmission factor 0.97): $E_d(\lambda, z)$ was measured at a depth that ranged from 6 to 10 m to avoid wave-induced focusing effects (15–20 m for the stations in clearer mesotrophic waters). The irradiance reflectance ratio is

$$R(\lambda) = E_u(\lambda, 0^-)/E_d(\lambda, 0^-).$$

$E_u(\lambda, 0^-)$ was inferred from $E_u(\lambda, \varepsilon)$ by extrapolation using the attenuation coefficient for upward irradiance ($K_u$) derived from deeper measurements. Note that lens-focusing effects do not affect the upward flux, and the signals were always very stable.

The CTD package included a rosette bottle sampling system for collecting seawater. The samples were collected along a vertical profile in close coincidence (less than 30 min) with the optical measurements. For some "fast" stations, only

Table 1
Relevant information regarding the BENCAL stations, which include the bio-optical measurements discussed here

| Station no. | Chl-surf ($mg\,m^{-3}$) | Bottom depth (m) | $Z_{eu}$ (m) | $a_y(380)$ ($m^{-1}$) |
|---|---|---|---|---|
| 1 | 11.300 | 27 | NA | 0.358 |
| 2 | 2.250 | 29 | X | 0.242 |
| 3 | 3.620 | 54 | X | NA |
| 4 | 2.640 | 53 | X | NA |
| 6 | 5.260 | 38 | X | 0.335 |
| 7 | 4.850 | 48 | X | 0.337 |
| 8 | 6.930 | 50 | | 0.439 |
| 10 | 6.250 | 32 | X | 0.339 |
| 11 | 3.890 | 44 | X | 0.421 |
| 12 | 4.410 | 93 | | 0.222 |
| 14 | 5.940 | 134 | | NA |
| 15 | 2.980 | 87 | | 0.127 |
| 16 | 2.910 | 154 | | 0.139 |
| 18 | 22.100 | 125 | | 0.164 |
| 19 | 29.100 | 132 | | 0.128 |
| 20 | 22.800 | 100 | | 0.128 |
| 21 | 8.150 | 100 | | NA |
| 22 | 0.520 | >400 | | <0.01 |
| 23 | 0.510 | >400 | | <0.01 |
| 26 | 0.245 | >400 | | 0.014 |
| 27 | 0.252 | >400 | | <0.01 |
| 29 | 1.170 | 163 | | <0.01 |
| 32 | 4.550 | 145 | | 0.067 |
| 33 | 9.390 | 128 | | 0.144 |
| 34 | 22.600 | 118 | | 0.109 |
| 37 | 5.380 | 98 | X | 0.175 |
| 38 | 2.030 | 107 | NA | 0.107 |
| 40 | 2.950 | 60 | NA | NA |
| 41 | 6.530 | 57 | X | 0.211 |

Successively (columns), station number, chlorophyll *a* concentration within the surface layer, bottom depth. Then (column denoted $Z_{eu}$), result of the application of the third criterion, which is based on the comparison of the depth of the euphotic layer ($Z_{eu}$) and the vertically integrated chlorophyll content (cf. Fig. 3); the crosses mean "identified as Case-2 water". Last column: absorption coefficient at 380 nm of the dissolved yellow substance (obtained through the inversion—see text). NA means not available.

surface samples were collected (bucket or pump) during the optical deployment. Several aliquots (ranging from 0.25 to 2.8 L) of the sample were filtered in parallel (25 mm GF/F filters) for several determinations. They include (i) the particle absorption spectrum, and the pigment concentration/composition, both carried out on the same filter; (ii) the mass concentration of suspended particulate material (SPM) on a second filter; and (iii) the particulate organic carbon concentration (POC) on a third filter.

The particulate absorption spectrum was determined from 375 to 750 nm (1 nm increment) by using another LI-COR instrument equipped with an integrating sphere, according to a method described in Lazzara et al. (1996). The correction for the pathlength amplification effect was made according to Bricaud and Stramski (1990). Following the absorption measurement, the filter was immediately frozen in liquid nitrogen, then stored at −80 °C for subsequent pigment HPLC analysis, made according to a slightly modified version of the method described by Vidussi et al. (2001), see also (Hooker et al., 2005). The total chlorophyll *a* concentration used hereafter, simply denoted (Chl), actually represents the sum of monovinyl-Chl-*a*, divinyl-Chl-*a*, and chlorophyllid-*a* concentrations. The ratio phaeophorbid-to-chlorophyll *a* was always found extremely low (<1%), which indicates active blooming conditions with a negligible presence of decomposition products.

Occasionally, the absorption spectrum was determined on duplicate samples, of which one filter was extracted according to Kishino et al.'s method (1985) for a measurement of the depigmented particles. In parallel, the numerical decomposition method (Bricaud and Stramski, 1990) was applied to all samples. By difference the contributions of phytoplankton ($a_\varphi$) and non-algal particulate matter ($a_{nap}$) to the total particulate absorption ($a_p$) can be determined. The $a_\varphi$ values from the BENCAL cruise, together with the detailed pigment composition and algal cell size, have already been discussed in Bricaud et al. (2004).

For the SPM determination, the cleaned filters were pre-weighed (micrometric balance MX5 Metler-Toledo) and stored in numbered Petri slides before use. After filtration and rinsing (distilled water), the filters were stored at −25 °C. They were then thawed in laboratory, dried at 45 °C, and re-weighed at room temperature. The particle mass on the filter was obtained by difference. For the POC determination, the GF/F filters were (before use) washed in a soxhlet with dichloromethane to remove carbon contamination without altering the filter porosity. The filtered volumes were between 0.5 and 2.5 L. Samples were analyzed using a PDZ Europa carbon–nitrogen analyzer with glycine as standard.

An absorption–attenuation meter (AC-9 manufactured by WETLabs) was operated as a bench-top instrument in a fixed tilt position (45°). To avoid bubble formation, it was gravimetrically filled from

below and using a tank (4 l) positioned above the AC-9. Only surface samples (the same as for SPM and pigment determinations) were measured in this fashion. Ultra-pure water (Milli-Q$^{TM}$) was regularly used for calibration (see details in Barlow et al., 2003). The standard temperature and salinity corrections were applied. The determination (at 9 wavelengths) of the attenuation and absorption coefficients allows the scattering coefficient to be obtained by difference.

In such high-Chl and patchy environments, where the conditions are rapidly changing as indicated by a continuous Chl-*a* fluorescence record, the operations were planned to ensure as well as possible a quasi-simultaneity of the sampling and optical determinations. Despite these cautions, some discrepancies due to temporal mismatch cannot be completely avoided. Emphasis was put on the properties of the near-surface layer in support of the satellite calibration/validation program.

## 4. Water identification

By analyzing field data collected in open ocean waters, the various optical properties can be studied in relation to (Chl) and average empirical relationships can be derived via regression analyses. This approach has a long history (e.g. Austin and Petzold, 1986; Baker and Smith, 1982; Gordon and Morel, 1983; Morel, 1988) and has been progressively refined with the increasing availability of data (e.g. Bricaud et al., 1995, 1998; Loisel and Morel, 1998; Sathyendranath et al., 2001; Staehr and Markager, 2004).

Actual field data are always scattered around the derived average relationships as a result of a natural variability, which does exist in Case-1 waters (Gordon and Morel, 1983; Gordon et al., 1988). This variability originates from possible changes in the relative proportions of the various components (algae vs. others, such as heterotrophic organisms, detritus, colored dissolved material) and from changes in the optical properties within each of the compartments (e.g., varying Chl-specific absorption by algae with pigment composition and cell size, or varying exponential slopes of the absorption by colored dissolved material). Despite their scatter, these relationships can be used as criteria to categorize waters into a Case-1/Case-2 scheme. In particular, Case-2 waters can be detected, as soon as significant departures with respect to the average relationships occur, which denote anomalous excess in absorption or scattering (or both). A "significant" departure is obviously a somewhat arbitrary notion. Four criteria will be employed.

### 4.1. Scattering coefficient and chlorophyll concentration

This criterion was initially introduced by Gordon and Morel (1983, their Fig. 5a) and revisited by Loisel and Morel (1998, their Fig. 3). It relies on the fact that the scattering coefficient at 550 nm, $b(550)$, and (Chl) are (rather loosely) co-varying in Case 1 waters. The presence of exogenous sediments (minerals in particular) increases the scattering coefficient, independently from algal cells and their retinue. Therefore a somewhat arbitrary threshold can be defined as an upper limit in $b(550)$ for a given (Chl) value. If $b$ is above this threshold, then the water is identified as "turbid Case-2" water. The upper limit for $b$ in Gordon and Morel (1983) was expressed as

$$b(550) = 0.45[\mathrm{Chl}]^{0.62}. \quad (1)$$

A recent and larger dataset was analyzed by Loisel and Morel (1998). Based on this analysis, the average relationship was slightly modified (Morel and Maritorena, 2001), becoming

$$b(560) = 0.416[\mathrm{Chl}]^{0.766}. \quad (1')$$

The scatter in the distribution of the $b$-(Chl) data for Case 1 waters (within a factor of ~3 around the average) suggests that a reasonable upper limit can be obtained by increasing the above coefficient (0.416) by 66%, without changing the exponent, so that the adopted threshold (see Morel and Belanger, 2006) is expressed as

$$b(560) = 0.69[\mathrm{Chl}]^{0.766}. \quad (2)$$

This criterion is slightly less severe than the previous one, in the sense that waters categorized as turbid Case-2 waters through the use of Eq. (1) may remain below the threshold defined by Eq. (2). In principle, $b$ in the above expressions is the particle scattering coefficient, $b_p = (b - b_w)$, where $b_w$ is the coefficient for water molecules (i.e. $0.0018\,\mathrm{m}^{-1}$ at 560 nm), here totally negligible compared to $b$. Only turbid waters can be identified in this way, owing to their high scattering, whereas highly absorbing waters (yellow substance dominated Case-2) are not detected. The field data are shown in Fig. 2a. A few stations, slightly above the upper limit as defined by Eq. (1), remain below the threshold

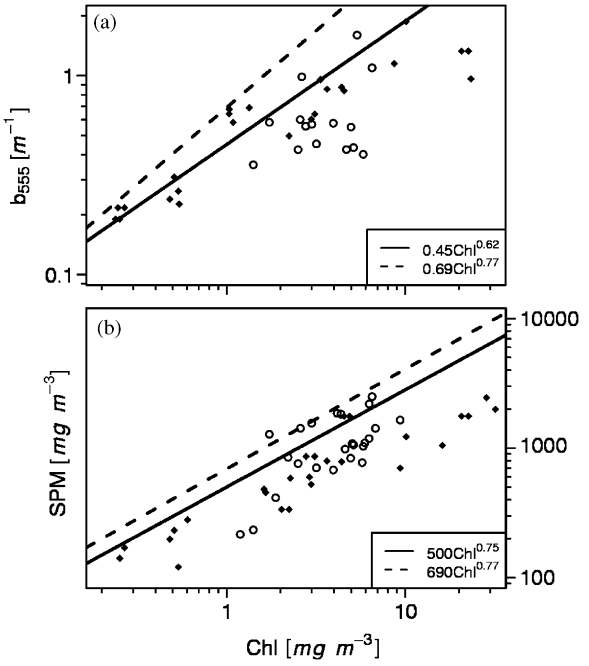


Fig. 2. (a) Scattering coefficient at 555 nm ($m^{-1}$) derived from the AC-9 measurements, as a function of the chlorophyll a concentration ($mg\,m^{-3}$) measured on the same near surface sample. The lines represent empirical relationships (see text and Eqs. (1) and (2)). Both scales are logarithmic. (b) Mass concentration of suspended particulate matter ($mg\,m^{-3}$) as a function of the chlorophyll concentration. Note that the data in this panel originate from the euphotic layer, and are thus more numerous than in panel a restricted to near surface samples. In both panels, black diamonds and circles are used as in Fig. 3 and correspond to stations of the Group 1 or 2 (see text).

expressed by Eq. (2). According to the somewhat arbitrary nature of the thresholds, a provisional conclusion could be that some stations are close to the margin of, without distinctly entering into, the turbid waters category.

### 4.2. Suspended particulate matter (SPM) and chlorophyll concentration

If the scattering coefficient and the SPM mass concentration were tightly related, a criterion based on SPM would be redundant with the previous one. Nonetheless, this information can be used because simultaneous determinations of (Chl) and SPM were also made in the past, independently from the scattering measurements, and statistically analyzed By considering mostly Case-1 waters, Clark et al. (1980) arrived at an average relationship

$$\mathrm{SPM} = 500[\mathrm{Chl}]^{0.75}, \tag{3}$$

where both SPM and (Chl) are expressed as $mg\,m^{-3}$. If the empirical relationship given in Gordon and Morel (1983, their Fig. 6), namely

$$\mathrm{SPM} = 1000b(550)$$

is combined with Eq. (1) or (2), it becomes

$$\mathrm{SPM} = 450[\mathrm{Chl}]^{0.62} \text{ or } \mathrm{SPM} = 690[\mathrm{Chl}]^{0.77}. \tag{4a),(4b)}$$

Several stations (Fig. 2b) are represented by data points above the line defined by Eq. (3), but are below the line defined by Eq. 4b (a less severe criterion). In conclusion, excessive particle loads, or highly turbid waters, are not detected.

### 4.3. Particulate organic carbon (POC)

The organic carbon content within the POC (as $mg\,m^{-3}$) brings complementary information about the composition of SPM. High SPM values compared to the POC content would denote the presence of mineral particles. This is not the case, as a linear regression between these two quantities provides the relationship

$$\mathrm{SPM} = 2.07\mathrm{POC}(0 \text{ intercept}, N = 49, r^2 = 0.91).$$

Five samples (Stations 2, 3, 4, 7 and 37) have been excluded from the regression analysis, with SPM/COP values ranging between 3 and 5. Actually, POC covaries with (Chl) in a rather regular (non-linear) manner for all stations (apart from Stations 7 and 37). The regression on the log-transform quantities leads to the relationship

$$\mathrm{POC} = 203(\mathrm{Chl})^{0.41} (N = 47, r^2 = 0.824)$$

similar to that found in less productive waters (Morel, 1988). The particulate material is thus essentially organic, dominated by phytoplankton and immediate derivatives, which is corroborated by the steady carbon-to-nitrogen ratio ($5.72 \pm 1.06$, $N = 73$). This conclusion agrees with the previous ones.

### 4.4. The column-integrated chlorophyll content and the depth of the euphotic layer

A purely empirical relationship was established in Case 1 waters (Morel, 1988) between the vertically integrated chlorophyll content of the euphotic zone ($\mathrm{Chl_{TOT}}$, $mg\,m^{-2}$) and the actual depth of this zone, $Z_{eu}$ (defined as that depth where the downward irradiance within the 400–700 nm band is reduced to

1% of its surface value). The depth $Z_{eu}$ was determined from the $E_d(\lambda, z)$ measurements. This average relationship has been recently revisited by Morel and Maritorena (2001) and supported by a spectral modeling approach (Morel and Gentili, 2004). It is numerically expressed as (when $Z_{eu} < 102$ m)

$$Z_{eu} = 912.5[\mathrm{Chl}_{TOT}]^{-0.839}. \quad (5)$$

Part of the scatter observed around this empirical relationship (about $\pm 15\%$ in $Z_{eu}$) is attributable to the dependence of $Z_{eu}$ on the sun's position (details and Fig. 1 in Morel and Gentili, 2004); the other part is due to the natural variability. For a given chlorophyll content, $Z_{eu}$ is reduced as soon as absorbing and (or) scattering substances, other than those normally present in Case 1 waters, occur in a significant amount. This criterion is thus more general than the previous ones, as it applies to both kinds of Case-2 waters (sediment-dominated or yellow-substance-dominated waters). If the observed $Z_{eu}$ is lower than the modeled (Eq. (5)) $Z_{eu}$ by 30% or more, the departure is considered as significant and thus identifies Case-2 waters. Consequently, the average coefficient (912.5) is replaced by its lower limit, namely by 638.

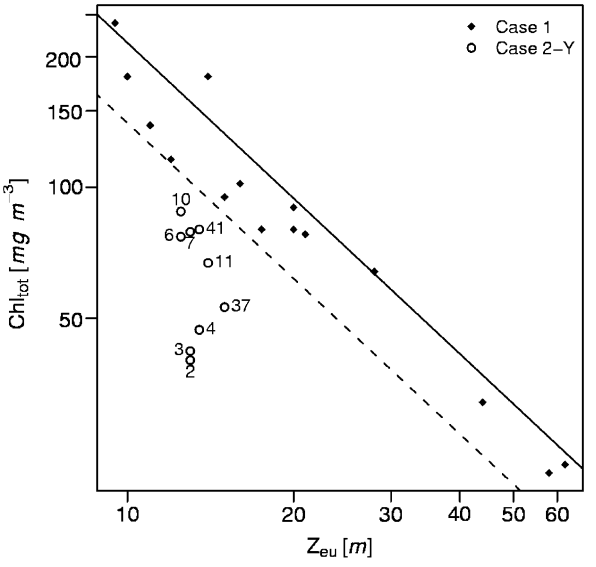


Fig. 3. Column chlorophyll content (mg m$^{-2}$) integrated from 0 to $Z_{eu}$ (euphotic depth) as a function of $Z_{eu}$ (m). The solid line represents Eq. (5), the dashed line represents the adopted lower limit. The empty symbols below the limit denote the Case-2-Y waters (see text and Table 1).

When sorting out the BENCAL results by applying this criterion (Fig. 3), 9 stations clearly depart from Case-1 waters (see Table 1). Those previously identified as being close to the upper limit in terms of turbidity (namely stations # 2, 3, 4, 37 and 41) are among these 9 stations. For all these stations, the cause of a significant reduction of $Z_{eu}$ is to be found in a larger content of yellow substance. This is supported by the fact that the absorption coefficient of dissolved yellow substance (at 400 nm), $a_y(400)$, exceeds 0.2 m$^{-1}$ at all these stations, while it is below this value for the others (S. Bernard, pers. commun.). A systematic exploitation of the $a_y$ data cannot be made, as they were often unreliably noisy (and close to the detection limit, 0.023 m$^{-1}$; Barlow et al., 2003). Nonetheless, the above values are high enough to be significant. Moreover, indirect $a_y$ determinations (displayed in Table 1), which will be presented later, corroborate the diagnostic of high yellow substance content.

### 4.5. Combined criteria and geography

The geographical distribution (Fig. 1) of the stations identified in Fig. 3 is perfectly consistent with their proximity to the coast and, maybe more importantly, with the bottom depth (< 50 m, Table 1). These stations are all located in St. Helena Bay, where a dense cover of kelp was often encountered (even to the point of perturbing the deepest samplings near the bottom). The departure from Case 1 conditions, which does not result from a significant resuspension of sediment, is rather caused by an enhancement of absorption due to yellow substance and (or) tiny colored detrital particles. These waters will be classified as "yellow substance dominated" (abbreviated as Case 2-Y). For convenience, in what follows the Case 1 waters will also be denoted by Group 1, the Case 2-Y waters by Group 2, and the four stations in offshore mesotrophic waters by Group 3. Emphasis will be put on the optical properties within the Group 1 and on their differences when compared to those of Group 2.

## 5. Results

### 5.1. Particle absorption at specific wavelengths

Empirical relationships (power functions) between the spectral absorption of the total (algal and non-algal) particulate matter, $a_p(\lambda)$, and (Chl)

were previously derived from field experiments in Case-1 waters (Bricaud et al., 1998) and are compared to the present data. The coefficients $a_p(442)$ and $a_p(676)$ at the two maxima in absorption are displayed as a function (Chl) (Figs. 4a and b). These $a_p$ values are remarkably well organized with respect to (Chl), which varies over 2 orders of magnitude. The present $a_p(442)$ values are on average about 50% above the mean relationship but stand within the range of possible variations for Case-1 waters (Bricaud et al., 1998). Similar excesses that are systematically observed at other wavelengths in the blue-green spectral domains (not shown), tend to decrease toward the red domain. For instance, the positive departure from the mean relationship is only ~15% at 676 nm. The stations of Groups 1 or 2 do not exhibit separate trends in Fig. 4, as the corresponding data are randomly distributed along the regression lines.

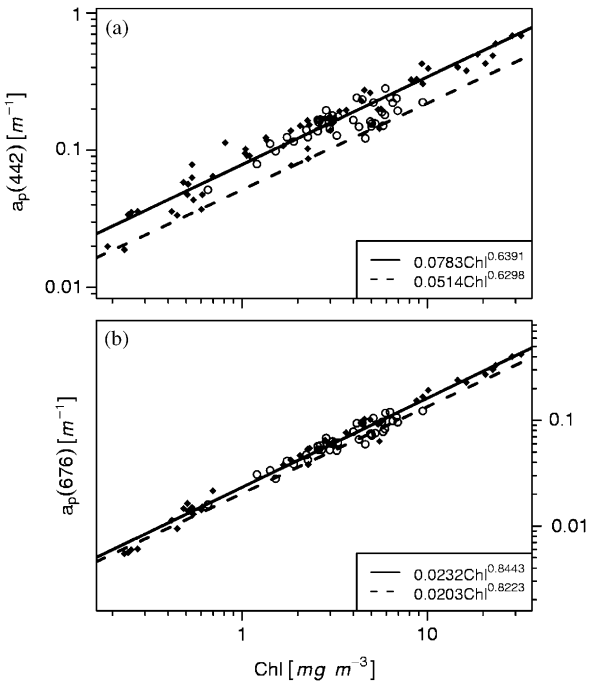


Fig. 4. Particle absorption coefficient ($m^{-1}$) as a function of the chlorophyll concentration determined on the same samples (in a log–log representation); (a) for the wavelength 442 nm, (b) for 676 nm. The samples are not restricted to the upper layer; they all belong to the euphotic layer. The solid straight lines represent the result of the linear regression between the (log-transformed) quantities, whereas the dashed lines represent the result of the regression performed by Bricaud et al. (1998). Black diamonds and circles are used (as in Fig. 3) and correspond to stations of the Group 1 or 2, respectively (see text).

### 5.2. Spectral shape of particle absorption within the 370–720 nm domain

For the first group (examples in Fig. 5a), the $a_p(\lambda)$ spectra are well featured, with the blue maximum prominently outlined and a distinct decrease from 440 nm toward 370 nm. These spectra tend to resemble those of pure algal cultures. The application of the methanol extraction method (Kishino et al., 1985) or the numerical decomposition technique (Bricaud and Stramski, 1990) allows the non-algal contribution to absorption to be quantified. For surface waters only, the ratios of the total particle absorption to the phytoplankton absorption, $a_p/a_\varphi$, at 400 and 440 nm, do not exceed one by a large amount for Group 1, and the average values

$$a_p(400)/a_\varphi(400) = 1.13(\pm 0.07, \text{at } 1\,\text{s}, N = 36),$$
$$a_p(440)/a_\varphi(440) = 1.058(\pm 0.064, \text{at } 1\,\text{s}, N = 36)$$

demonstrate that the non-algal contribution is rather low. When Group 2 is considered (examples in Fig. 5b), a noticeable difference occurs in the UV domain, where absorption remains high. In the visible part of the spectrum, the mean $a_p/a_\varphi$ ratios are notably enhanced

$$a_p(400)/a_\varphi(400) = 1.34(\pm 0.16, \text{at } 1\,\text{s}, N = 22),$$
$$a_p(440)/a_\varphi(440) = 1.15(\pm 0.08, \text{at } 1\,\text{s}, N = 22),$$

which suggests that colored detritus produces an additional absorption in the short wavelength domain. This increase cannot be ascribed to a degraded form of chlorophyll, as for all samples (two groups merged) the ratio pheophorbid-to-chlorophyll *a* was always extremely low (see above).

For Group 1, and even for Group 2, the relative contribution of non-algal particles, (i.e. the quantity $(a_p - a_\varphi)/a_p$) is small (6–15%), significantly below the average value observed in meso- or oligotrophic Case 1 waters (amounting to ~35% at 440 nm, see Fig. 2b in Bricaud et al., 1998). At least in the Benguela upwelling zone, and in this season, the particulate absorption is largely dominated by living cells, while derived detritus seem to play a limited role. This is no longer true in the offshore mesotrophic waters (see below).

As expected, the chlorophyll specific particle absorption values, $a_P^*(\lambda)$, i.e. $a_p(\lambda)/(\text{Chl})$, are generally low. As inferred from Fig. 4a, $a_P^*(442)$ decreases regularly with increasing (Chl) from ~0.07 $m^2\,mg^{-1}$ (when (Chl)~1 $mg\,m^{-3}$) to ~0.02 $m^2\,mg^{-1}$ (when (Chl) > 20 $mg\,m^{-3}$). Such values reflect

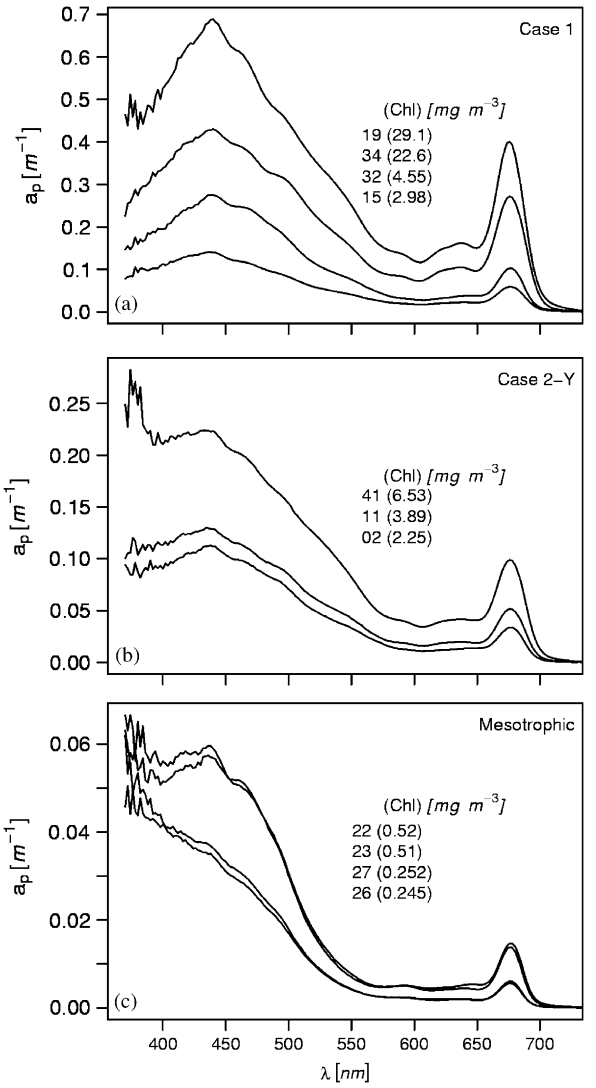


Fig. 5. Examples of particulate absorption spectra ($m^{-1}$) for samples from the near surface layer, (a) Group 1, (b) Group 2, and (c) Group3 (mesotrophic Case 1 waters). The station numbers are indicated and ordered from top to bottom as the spectra; the chlorophyll concentrations are also indicated (between parentheses). Note the change of scale for the ordinate axes.

the pigment packaging effect that increases with (Chl). This is fully compatible with the predominance in high (Chl) waters of microphytoplankton, as revealed by the high proportions of fucoxanthin and peridinin in most of these samples (see discussion in Bricaud et al., 2004; also Bernard et al., 2001).

Eight absorption spectra (four of them are displayed in Fig. 5c) for the offshore mesotrophic waters are excluded from the $a_p/a_\varphi$ average ratios given above. Their ascending slopes toward UV, and high values in this domain, denote a high relative abundance of detritus in these "clear" waters. The $a_p^*(\lambda)$ values in the blue are also much higher (by a factor of 3) than in Groups 1 and 2; they are typical of smaller phytoplankters, as supported by the pigment composition (discussed in Bricaud et al., 2004).

### 5.3. Attenuation coefficient for downward irradiance, compared to modeled values

The $K_d(\lambda)$ spectra examined below deal exclusively with the upper layer. As this attenuation coefficient is roughly a "proxy" of the absorption coefficient (Gordon, 1989), these $K_d(\lambda)$ spectra have much in common with $a_p(\lambda)$, at least within the spectral domain where absorption is not dominated by the water absorption ($\lambda < 580$ nm). Consistently, the $K_d(\lambda)$ spectra for Group 1 (Fig. 6a, to be compared to Fig. 5a) exhibit also a distinct minimum near 370 nm. In contrast, for Group 2 (Fig. 6b, to be compared to Fig. 5b), the UV minimum disappears and is replaced by a regularly ascending slope from 560 to 320 nm. Compared to the $a_p(\lambda)$ spectrum (Fig. 5b), a difference appears in the near UV. Indeed, although the $a_p(\lambda)$ spectrum decreases slightly from 437 to 380 nm, the $K_d$ values steadily increase, because the yellow substance absorption contributes to the diffuse attenuation.

The $K_d(\lambda)$ field data were studied (Morel 1988, Morel and Maritorena, 2001) by using this approximation, which involves considering $K_d(\lambda)$ as the sum of a term for pure water ($K_w$) and a term merging the contributions of all biogenic, optically significant, components (algal cells and all associated particulate and dissolved non-algal materials), denoted $K_{bio}$,

$$K_d(\lambda) = K_w(\lambda) + K_{bio}(\lambda) \quad (6)$$

with

$$K_w(\lambda) = a_w(\lambda) + (1/2)b_w(\lambda), \quad (7)$$

where $a_w$ and $b_w$ stand for the absorption and scattering coefficients of optically pure sea water, respectively. Then, by carrying out a regression analysis on $K_{bio}(\lambda)$ and (Chl) (on their log-transform), power laws of the form

$$K_{bio}(\lambda) = \chi(\lambda)[\mathrm{Chl}]^{e(\lambda)} \quad (8)$$

were derived. When the Bencal data are superimposed on previous $K_{bio}$ data (examples in Figs. 7a

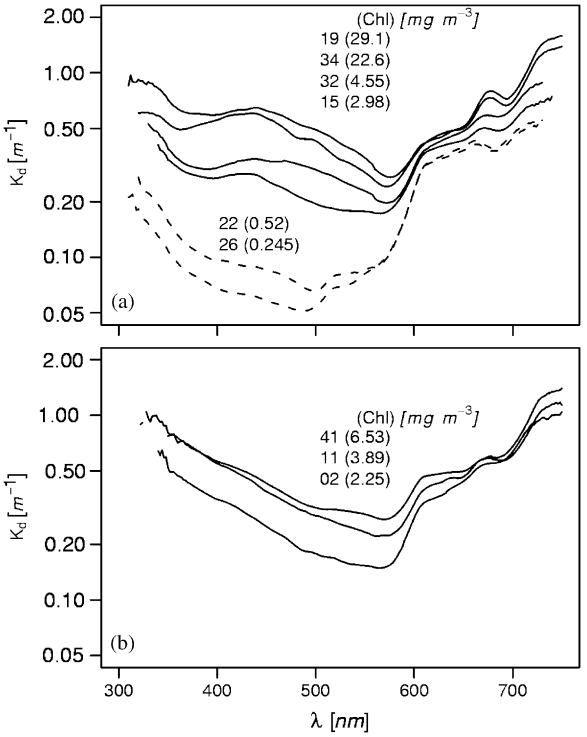


Fig. 6. Examples of the spectral values of the diffuse attenuation coefficient for downward irradiance, $K_d(\lambda)$, (as $m^{-1}$), (a) in Case 1 waters and (dashed curves) in mesotrophic Case 1 waters , (b) in Case-2-Y waters. The stations numbers and (Chl) are indicated and ordered from top to bottom as the spectra.

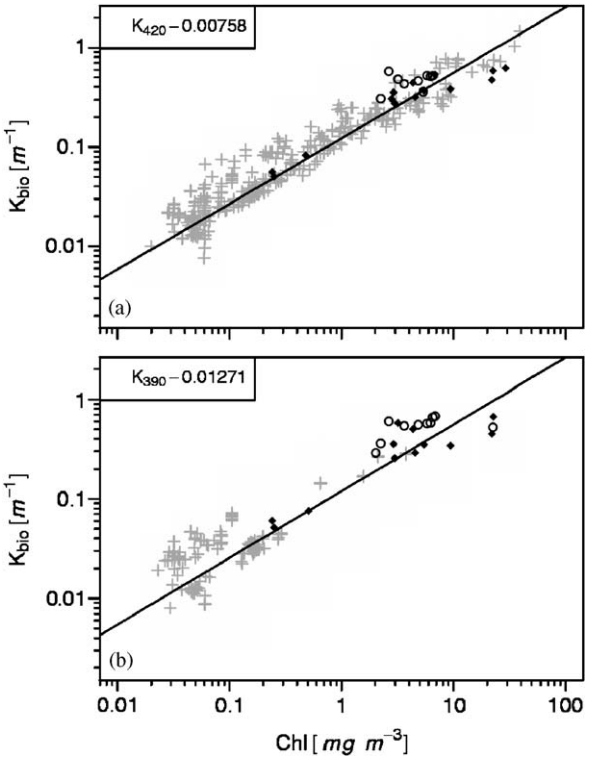


Fig. 7. Log-log plot of $K_{bio}$ (Eq. (6)) as a function of (Chl); (a) for the wavelength 420 nm, and (b) for 390 nm. The data with gray symbols are reproduced from the Figs. 3 and 7 in Morel and Maritorena (2001), on which the present data (symbols as in Figs. 2–4) are superimposed.

and b), the general trend is not altered. The data for Group 1 are scattered around the average regression line, whereas the data for Group 2 are slightly above the regression line. This difference between the two groups, as detected in the short wavelengths domain (390 and 420 nm), tends to vanish in the green part of the spectrum (not shown).

A separate regression between $K_{bio}(\lambda)$ and (Chl) has been carried out on the Bencal dataset (all data merged, regardless of their status). The resulting $\chi(\lambda)$ and $e(\lambda)$ parameters slightly differ from those in Morel and Maritorena (2001). In the restricted range of high (Chl), however, the Bencal-specific and the previous regression lines are very close. This is illustrated (Fig. 8) by using these Bencal-specific parameters to produce the average $K_{bio}$ spectrum for (Chl) = 10 mg m$^{-3}$. It agrees with the spectrum (redrawn from Fig. 4c, in Morel and Maritorena, 2001) derived from the previous parameterization used at its limit of validity. The behavior of $K_{bio}$ for higher (Chl), and in the UV domain, beyond the limits of the previous parameterizations, can now be described.

### 5.4. Spectral shape of the particle scattering

The AC-9 instrument provides the optical coefficients $a_{tot}$ ( $= a - a_w = a_p + a_y$), and $c_{tot}$ ( $= c - c_w = a_p + a_y + b_p$), where $a_y$ denotes the absorption by yellow substance. The particle scattering coefficients, $b_p(\lambda)$, were determined at 9 discrete wavelengths from 412 to 715 nm as the difference ($c_{tot} - a_{tot}$). The $c_{tot}$ spectra were generally featureless, with an ascending slope toward the short wavelengths (not shown). The $a_{tot}$ spectra exhibited the absorption features of phytoplankton with peaks at 440 and 676 nm (or in Group 2 a regular increase between 440 and 412 nm). As a result of the ($c_{tot} - a_{tot}$) subtraction, the spectral shapes of scattering and absorption appear to be rather complementary. It is only approximately true, as theoretical computations show that a minimum in scattering does not necessarily coincide with a maximum in absorption (at least for algal cells, see Bricaud and Morel, 1986). The nine discrete channels of the instrument cannot resolve such possible spectral shifts.

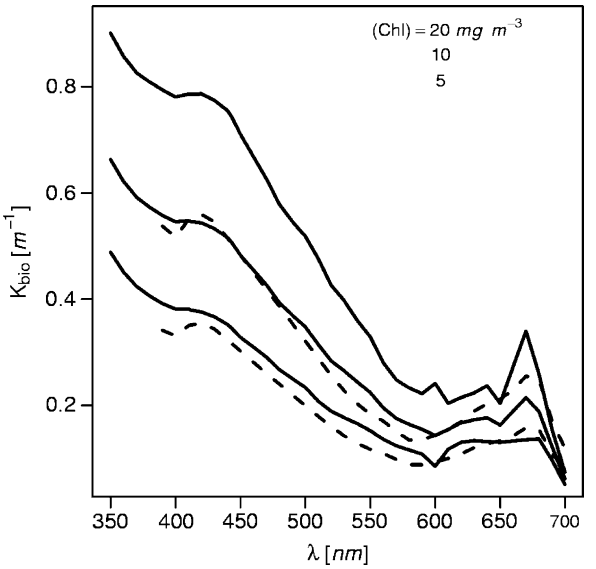


Fig. 8. Solid curves: spectral values of $K_{bio}$ when (Chl) = 5, 10, and 20 mg m$^{-3}$, as derived from the present study; the dashed curve for 10 mg m$^{-3}$ is reproduced from Fig. 4 in Morel and Maritorena (2001), and the dashed curve for 5 mg m$^{-3}$ is produced by the same model (Morel and Maritorena, 2001).

To study the spectral shape of $b_p(\lambda)$, the coefficients are normalized with respect to the spectrally averaged coefficient $[b_p]$, computed as (trapezoidal integration between 412 and 715 nm)

$$[b_p] = (1/303)\sum_{n=1}^{n=9}[b_p,(n) + b_p(n+1)][\lambda(n+1) - \lambda(n)]/2, \quad (9)$$

where $b_p(n)$ is the $b_p$ value in the $n$th channel of the instrument centered on $\lambda(n)$.

The first Fig. (9a) deals with Group 1 (average (Chl) value 8.9 mg m$^{-3}$, non-Gaussian distribution). The depressive effect of the pigment absorption bands (at 440 and 676 nm) on the scattering coefficient is clearly seen on these spectra. The most affected ones are those with the highest chlorophyll concentration and the "purest" algal populations (stations 18, 19, and 34). For moderate (Chl), the spectra are less affected by absorption and resemble those shown in Babin et al. (2003) for Case 1 waters (their Fig. 3a and 11). Fig. 9b deals with the Group 2 (average (Chl) value 5.52 mg m$^{-3}$). The general shape is quite different. While the trough around 675 nm is still well marked, a systematic and rather regular ascending slope toward the short wavelengths replaces the minimum of the previous figure. This slope (also for the mesotrophic waters in Fig. 9b) approximately corresponds to a $\lambda^{-0.6}$ dependency.

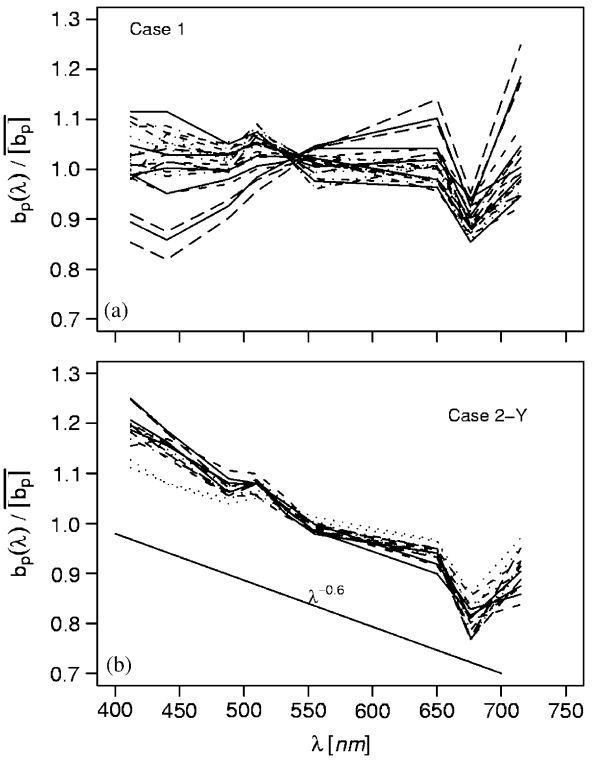


Fig. 9. Spectral values of the scattering coefficients normalized by their spectrally averaged coefficient (Eq. (9)). The center wavelengths of the AC-9 instrument are 412, 440, 488, 532, 555, 676, and 715 nm (bandwidth of 10 nm). All available data are represented. (a) Case 1 waters, (b) Case 2-Y waters plus mesotrophic waters (thin dotted curves).

### 5.5. Reflectance $R(\lambda)$

If the backscattering was spectrally neutral, the reflectance spectra would be inverted images of the $K_d$ spectra. This approximation allows the main features of the reflectance spectra to be understood.

Typical examples from Group 1 are shown in Fig. 10a. For high (Chl), the remarkable feature is the doubled peak structure. Besides the usual maximum at 570 nm, a second maximum appears in the UV domain, around 360–370 nm, which has not been previously described. Between these two peaks, the minimum at 437 nm reflects as usual the algal (chlorophylls plus carotenoids) absorption maximum. The second reflectance minimum, near 664 nm, corresponds specifically to the Chl-*a* absorption maximum (occurring at 676 nm). The shift from 676 to 664 nm is the consequence of the

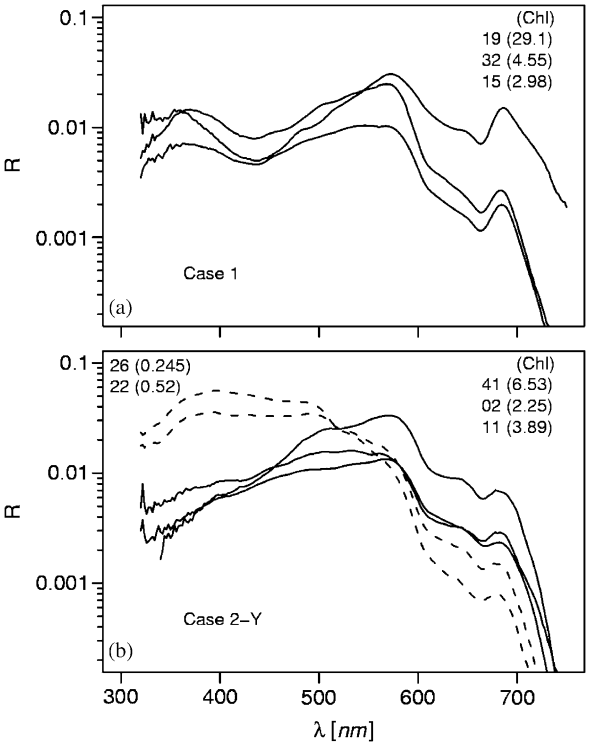


Fig. 10. Irradiance reflectance spectra for some selected stations. (a) Case 1 waters, (b) Case 2-Y waters, and mesotrophic waters (dashed curves). The station numbers and (Chl) are indicated and ordered from top to bottom as the spectra.

presence of the prominent chlorophyll *a* fluorescence peak (centered on 687 nm), which partially overlaps, and thus distorts, the minimum (see e.g. Gower et al., 1999). The remarkable change in Group 2 (Fig. 10b) is the disappearance of both the minimum at 437 nm and the maximum around 365 nm. These features are replaced by a convex shape between the maximum (at 570 nm) and the UV domain. At larger wavelengths (>500 nm), the spectral shapes are similar for both groups.

## 6. Discussion

The inherent optical properties are in principle derivable from the determination of upward and downward irradiance. Various solutions of this inverse problem have been thoroughly reviewed (Gordon, 2002). A simple inversion, based on the apparent optical properties $K_d$ and $R$, can be performed. These (apparent) properties can be related to the absorption and the backscattering coefficients, $a$ and $b_b$, respectively, through

$$K_d(\lambda) = 1.0395[\mu_d(\lambda)]^{-1}[(a(\lambda) + b_b(\lambda)], \quad (10)$$

$$R(\lambda) = f'[b_b(\lambda)/[(a(\lambda) + b_b(\lambda)], \quad (11)$$

where $\mu_d$ is the average cosine of the downward irradiance below the surface, and $f'$ is a dimensionless factor depending on illumination conditions and water properties. Both equations were obtained through numerical simulations of the radiative transfer within oceanic waters (Gordon, 1989; Gordon et al., 1975; Morel and Gentili, 2004). When solved for $a$ and $b_b$, the above equations provide the desired coefficients

$$a(\lambda) = 0.962K_d(\lambda)\mu_d(\theta_s, \lambda, \text{Chl}) \times [1 - R(\lambda)/f'(\theta_s, \lambda, \text{Chl})], \quad (12)$$

$$b_b(\lambda) = 0.962K_d(\lambda)\mu_d(\theta_s, \lambda, \text{Chl}) \times [R(\lambda)/f'(\theta_s, \lambda, \text{Chl})]. \quad (13)$$

Both $\mu_d$ and $f'$ actually depend on the sun position (the zenith sun angle, $\theta_s$) and on the water optical properties which vary with (Chl) and $\lambda$. The quantities $\mu_d$ and $f'$ have been theoretically studied for clear sky conditions (Morel et al., 2002), and lookup tables have been produced with (Chl), $\lambda$, and $\theta_s$ as entries (available over the internet, using anonymous ftp from oceane.obs-vlfr.fr, cd pub/morel, files f,fprime,mud).

For each station, $\theta_s$ is computed (ranging from 21°30 to 57°45); the measured near-surface chlorophyll concentrations are known, so that the above equations can be numerically solved, with the appropriate $\mu_d$ and $f'$ values. For this inversion, the lower limit of the spectral domain is 350 nm, and the upper limit is 600 nm, because inelastic processes (Raman scattering and chlorophyll fluorescence) affect both the reflectance and the attenuation values beyond this wavelength. No attempt to correct for these effects was made here.

It is worth noting that the main term in the evaluation of the absorption coefficient is $K_d$, because $R$, which is a rather small number, intervenes as a corrective term (inside the bracket). In the evaluation of $b_b$, the situation is quite different, as $K_d$ and $R$, through their product, play equivalent roles. This remark has practical consequences. Indeed, the uncertainties on these radiometric quantities, essentially due to the uncertainties on the measurement depth (see Section 3), are not equivalent. For $K_d$, which is determined between the surface and a certain depth $Z$, the uncertainty is expressed by $\Delta Z/Z$ (where $\Delta Z$ is the depth uncertainty). Therefore $K_d$ is easily determined within a $\pm 10\%$ interval. The $R$ values at null depth

(0−) are derived from $E_u$ values determined at a certain minimal depth, $\varepsilon$, which is not precisely known ($\pm\Delta\varepsilon$). The extrapolation of $E_u(\varepsilon\pm\Delta\varepsilon)$ to obtain $E_u(0-)$, and thereafter $R$, entails an uncertainty within a range expressed by the factor exp $[K_u(\pm\Delta\varepsilon)]$. This uncertainty may be considerable in adverse sea conditions and strongly absorbing waters. For instance, it is within a range (−23%, +28%) if $\Delta\varepsilon = \pm 0.5$ m and $K_u = 0.5\,m^{-1}$. As $K_u$ increases toward the UV part of the spectrum, the uncertainty is larger in this spectral domain. In summary, the inversion can be made rather accurately for the absorption coefficient, but significantly less accurately for the backscattering coefficient, particularly in unfavorable sea surface conditions. Note that if the uncertainty on $b_b$ is large, no systematic bias is to be expected, as the sign affecting $\Delta\varepsilon$ is at random.

### 6.1. Total absorption

The total absorption coefficient ($a_{tot}$), as obtained through the inversion of the AOPs (Eq. (12)), accounts for all absorbing substances (water, particulate and dissolved materials). Once the absorption coefficient for water molecules, $a_w$, has been subtracted from $a_{tot}$, the result (i.e., $(a_{tot}-a_w) = (a_p + a_y)$, where $a_y$ represent absorption by yellow substance) is directly comparable to the measurement carried out with the bench-top AC-9 instrument (Fig. 11a). Apart from the lowest values (too close to that of water), the agreement is excellent (slope 1.07, intercept −0.02, rms 0.05), especially when it is considered that the sampling and the in situ measurements were never perfectly simultaneous, and also when accounting for uncertainties attached to both the in vitro measurements and AOP inversion.

At the same wavelengths, another comparison can also be made with the particle absorption, $a_p$ (filter pad method). A positive difference between $(a_{tot}-a_w)$ and $a_p$ is now expected, in particular for the short wavelengths (412 and 440 nm), as a result of the absorption by the dissolved yellow substance. This difference is clearly seen on Fig. 11b, and, as anticipated, is more accentuated for Group 2.

Finally the $(a_{tot}-a_w)$ values can also be compared with the $(a_{mod}-a_w)$ values, where $a_{mod}$ stands for the modeled values computed by operating the Morel and Maritorena model (2001) with the actual (Chl) values (Fig. 11c). Since the model (based on $K_{bio}$) inherently accounts for the presence in Case 1

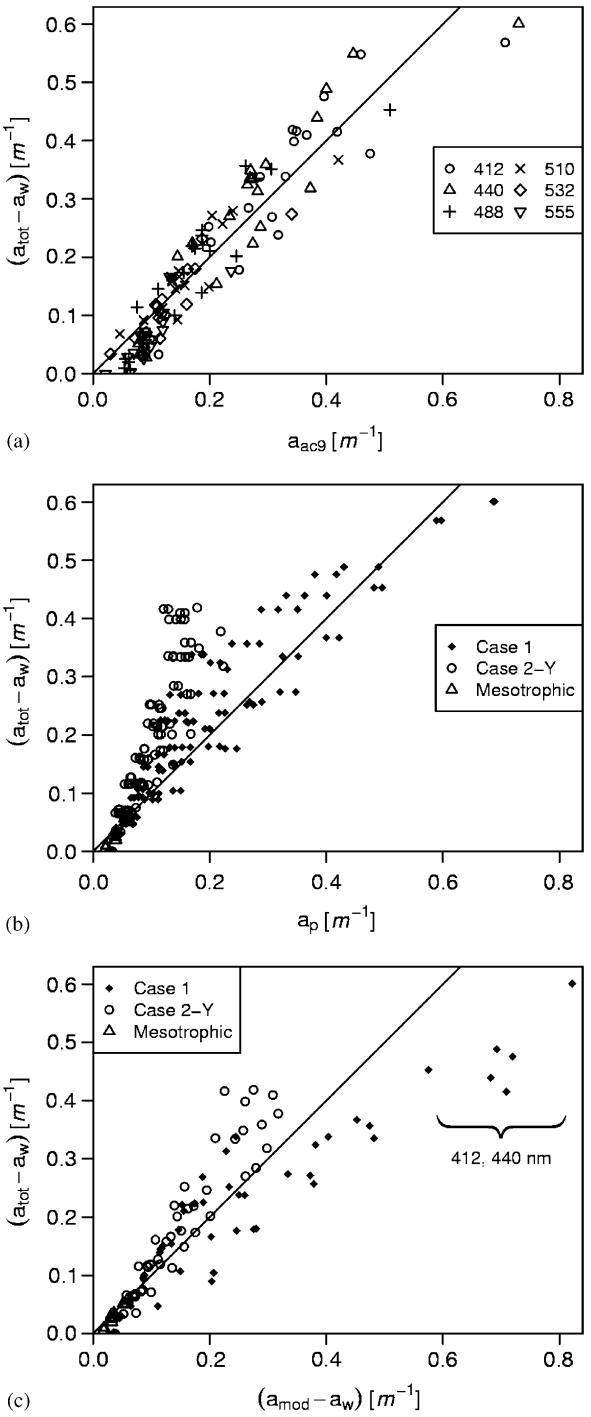


Fig. 11. Computed total absorption values (Eq. (11)) minus the absorption coefficient for pure water, i.e., the quantity $(a_{tot}-a_w)$, as a function of the AC-9 measured values at the 6 discrete wavelengths below 600 nm (in (a)); as a function of the particulate matter absorption (in (b)); as a function of the absorption modeled from the chlorophyll concentration (in (c)). Note that some $(a_{tot}-a_w)$ values may become slightly negative for the green wavelengths and in the case of weakly absorbing mesotrophic waters.

waters of a certain "average" amount of yellow substance associated with phytoplankton, no difference is expected. Actually, the field values (at 412 and 443 nm) are below the modeled ones, particularly for the highest (Chl) values (beyond the domain of model applicability). The extrapolation of the model leads to an overestimation of the yellow substance content. Within Group 2, with more yellow substance, the field values logically must (and do) exceed the modeled values.

The differences in the near UV domain between $a_p$ and $(a_{tot}-a_w)$ are evidenced by Fig. 12a and b, where several couples of spectra are displayed for a visual comparison. In addition, the corresponding yellow substance absorption spectra, obtained as $a_y = (a_{tot} - a_w - a_p)$ are also shown (Fig. 12c). These computations, when systematically effected, lead to the $a_y(380)$ values listed in Table 1, which confirm the previous identification of the Case 2-Y waters.

A global quantitative comparison is obtained by plotting (Fig. 13a and b) all the $(a_{tot}-a_w)$ values as a function of (Chl), together with the regression lines already obtained for $a_p$ (as in Fig. 4). On average (3 groups merged), the $(a_{tot}-a_w)$ values exceed the $a_p$ values by ~50% at 400 nm, and by ~30%, at 442 nm. The $(a_{tot}-a_w)$ values for the Case 2-Y waters are, as anticipated, systematically above those of Case1 waters, and above the average.

### 6.2. Backscattering coefficient

The backscattering spectra are displayed on Figs. 14a–c. Many of the spectra of the first group include a notable depression in the 440 nm region, which is especially pronounced for the highest (Chl) (St 19, 20, and 34, Fig. 14a). This feature will be analyzed later. In contrast, for Group 2 (and for the mesotrophic waters), the spectra are rather featureless. It is worth noting that the effect of water molecules through $b_{bw}(\lambda)$ (the pure seawater backscattering coefficient) is far from being negligible in the backscattering process, even for such heavily loaded waters. The particle backscattering coefficient, $b_{bp}(\lambda)$ can be computed as the difference $b_{bp}(\lambda) = b_b(\lambda) - b_{bw}(\lambda)$. The $b_{bp}(550)$ coefficients are plotted as a function of (Chl) for all stations (Fig. 15a). In spite of a considerable scatter, the general trend is clear, and $b_{bp}(550)$ increases by one order of magnitude when (Chl) spans two orders of magnitude. This increase coincides with the empirical covariation with $(Chl)^{0.5}$, as

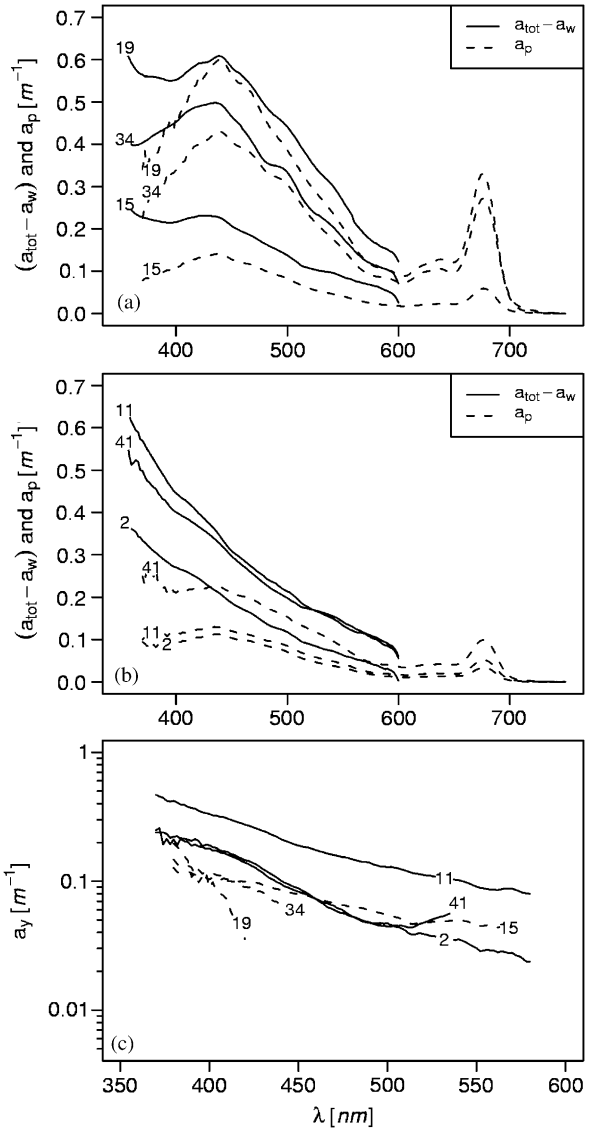


Fig. 12. Spectra of $(a_{tot}-a_w)$ compared to the spectra of particle absorption coefficient, $a_p$, for selected stations in Case 1 waters (a), and in Case 2-Y waters (b). The spectra of $a_y$, obtained by difference $(a_{tot}-a_w-a_p)$, are shown in (c); the solid curves are for Case 2-Y and the dashed curves for Case 1 waters, respectively; note that in the latter case, the difference may become insignificant.

observed by Stramska et al. (2003), and agrees with the parameterization of Morel and Maritorena (2001).

The featureless $b_b$ spectra for Group 2 are (Fig. 14b) parallel to the spectrum of the molecular backscattering, which suggests that the particle backscattering is spectrally quasi-neutral. More insight can be gained by examining the particle

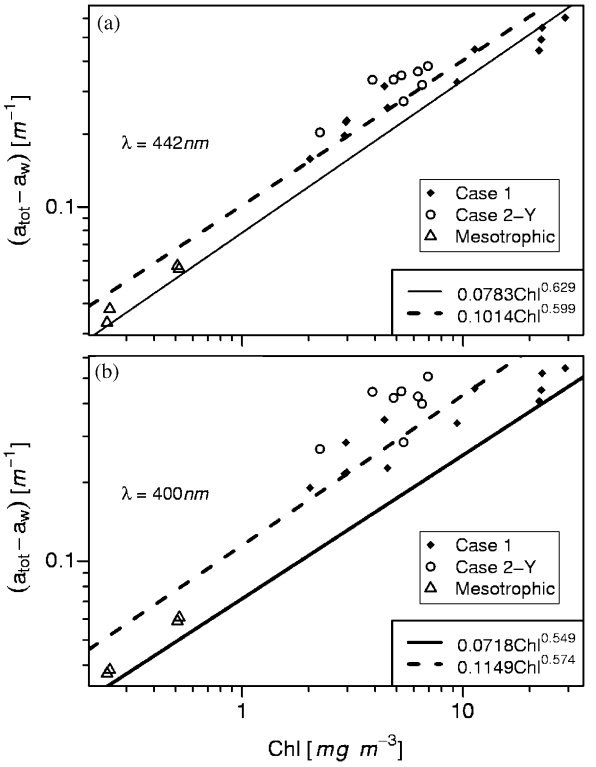


Fig. 13. Computed values of the absorption coefficient minus that of pure water, ($a_{tot} - a_w = a_p + a_y$), at the wavelengths 442 and 400 nm plotted as a function (Chl) for all Bencal stations (symbols as in Figs. 2–4). The dashed lines represent the regression for these data; the solid lines represent the regression for the particle absorption coefficient ($a_p$, as in Fig. 4); the equations for these lines are also indicated.

backscattering efficiency, $\tilde{b}_{bp}$,

$$\tilde{b}_{bp} = b_{bp}/b_p.$$

The particle scattering coefficient $b_p$ is provided by the AC-9 measurements (at the six wavelengths $<600$ nm). The computed efficiencies (displayed on Fig. 15b) do not show any notable wavelength dependency, except perhaps a decreasing trend toward the shorter wavelength. This trend can also be seen (Fig. 15c) for the mean values, separately computed for the two groups. Both theoretically and experimentally, it was shown (Ahn et al., 1992) that the backscattering efficiency of algal cells (at least of large cells, and in pure culture) may experience a minimum within the blue absorption band. The slight $\tilde{b}_{bp}$ decrease in the blue part of the spectrum likely results from this effect, which, however, remains minor.

After averaging over all wavelengths, the $\tilde{b}_{bp}$ values are lower for Group 1 than for Group 2

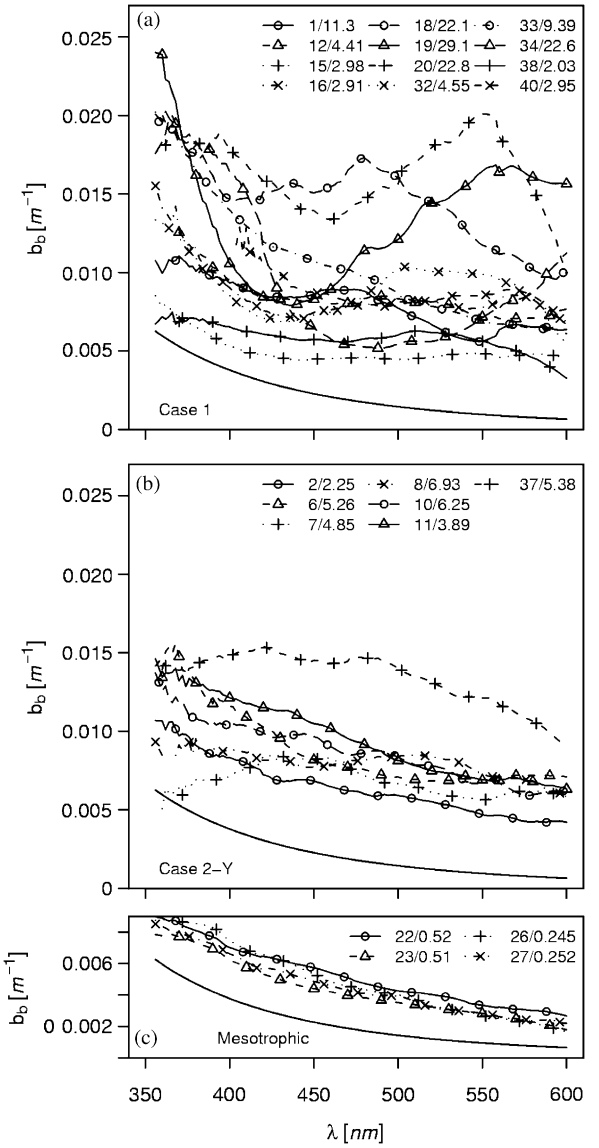


Fig. 14. Spectra of the total backscattering coefficient (Eq. (12)). All stations are represented and the three panels are for Case 1, Case 2-Y, and mesotrophic waters as indicated; the backscattering spectrum of pure water is reproduced in each panel (curve without symbol).

(0.80% vs 1.25%). This difference could indicate that the relative abundance of tinier (and perhaps more refringent) particles is higher in Case 2-Y waters than in Case 1 waters dominated by algal material. Such efficiencies, around 1%, are within the range of those recently observed (Twardowski et al., 2001; Boss et al., 2004; Sullivan et al., 2005) and imply that organic particulate material with low relative refractive index (1.04–1.08) largely dominates the particle population. A result clearly

emerges. Since the spectral dependency of $\tilde{b}_{bp}$ is limited, the pronounced features of the backscattering spectra (Fig. 14a) essentially originate from those already existing in the scattering spectra (Fig. 9).

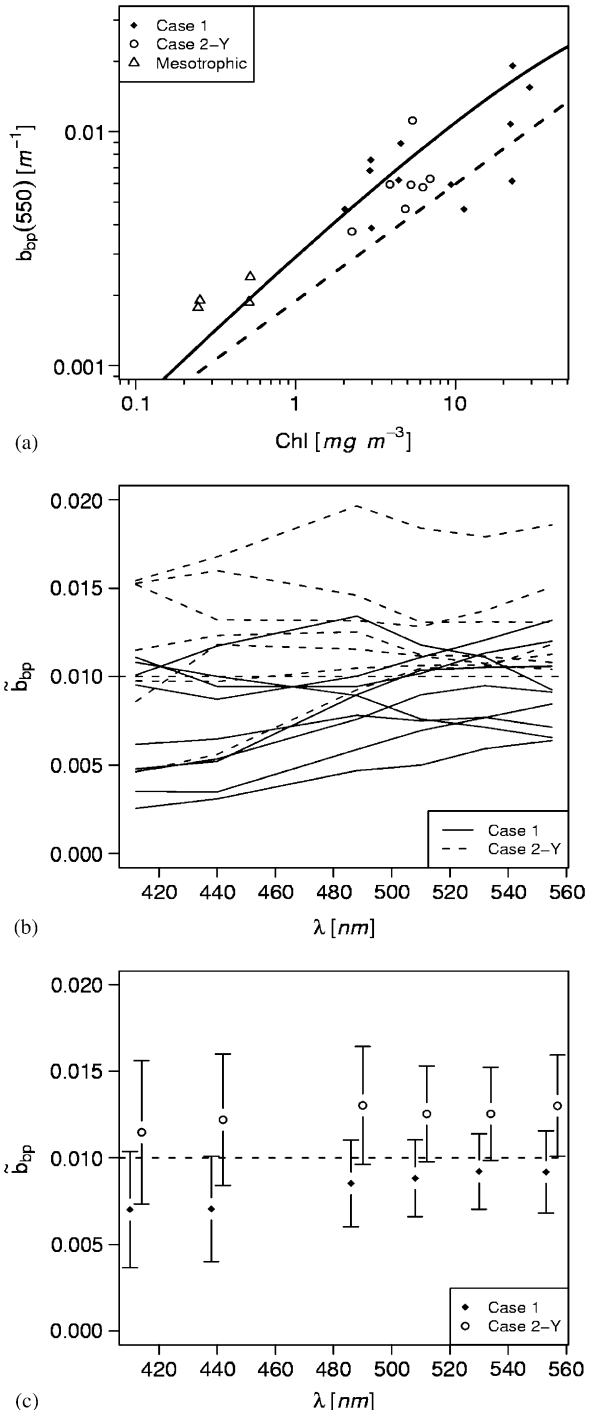


Fig. 15. (a) Particulate backscattering coefficient as a function of the chlorophyll concentration for all stations; the dashed straight line represents the empirical equation derived by Stramska et al. (2003, their Eq. (13a)) for Arctic waters, the solid curve the parameterization proposed by Morel and Maritorena (2001, their Eq. (13)). (b) Examples of backscattering efficiency of the particulate material, $\tilde{b}_{bp} = (b_b - b_{bw})/b_p$, computed at the wavelengths of the ac-9 measurements; the spectra are drawn by linear interpolation. (c) Mean values of $\tilde{b}_{bp}$, separately computed for all the stations of the Groups 1 and 2, at the wavelengths of the ac-9 measurements. The vertical bars represent the standard deviation. For clarity, a small shift in wavelength is introduced to separate the two groups.

These mean $\tilde{b}_{bp}$ values (Fig. 15c) exceed by about 50% those modeled by Eqs. (13)–(14) in Morel and Maritorena (2001) for similar chlorophyll concentration, and are well above those derived from theoretical considerations presented by Ulloa et al. (1994). They also are higher than those produced by the empirical relationship proposed by Twardowski et al. (2001, their Eq. (17)), albeit staying inside the envelope of their field data (their Fig. 11). They agree better with the expression proposed by Sullivan et al. (2005, their Eq. (6)). When plotted as a function of (Chl), the individual $\tilde{b}_{bp}$ values do not exhibit any trend (not shown). The present data as well as those of the above referenced studies demonstrate the high variability in the particle backscattering process and the difficulty of proposing an adequate parameterization.

### 6.3. Irradiance reflectance and ocean color algorithms

The magnitude of the irradiance reflectance at 560 nm is examined first. Indeed, $R(560)$ can be used when processing remotely sensed ocean color in view of identifying coastal turbid zones, where the chlorophyll concentration is in general wrongly estimated (Bricaud and Morel, 1987; Morel and Belanger, 2006). The $R(560)$ values for the Bencal cruise are plotted (Fig. 16a) as a function of (Chl), together with data previously collected in Case 1 waters in other parts of the world ocean (including a few from other upwelling areas). They corroborate the general trend previously observed in the domain of moderate (Chl). The solid curve represents an upper limit computed by using the upper value of the scattering coefficient (Eq. (2)) in combination with the reflectance model (Morel and Maritorena, 2001), and for a sun–zenith angle set at 45° (Eq. 11). Therefore, reflectance data above this threshold

would indicate that the corresponding water is of the sediment-dominated Case 2 water type. The Bencal values are well below this threshold, and there are no such waters in the studied zone. This conclusion is supported by the fact that "turbid flags" applied to the SeaWiFS and MERIS scenes (not shown) are not raised in this area.

To interpret the ocean color data in Case 1 waters, the algorithms (empirical or semi-analytical) in current use are based on the values of blue-to-green ratios (of normalized water-leaving radiances or of reflectances) which are related to (Chl). For instance, for the MERIS sensor (similarly to the SeaWiFS sensor), the successive $r$-ratios (see legend, Fig. 16b) in use for increasing (Chl) are $R(443)/R(560)$, $R(490)/R(560)$, and $R(510)/R(560)$, and a unique polynomial connects the three ratios. It is worth noting that this polynomial does not result from a best fit between reflectance and (Chl) data, simultaneously determined in the field (as is the case for the empirical OC4V4 algorithm in use with SeaWiFS; O'Reilly et al., 1998) but results instead from the semi-analytical approach, developed in Morel and Maritorena (2001).

Apart from the mesotrophic waters, most of the Bencal data are in the domain of high (Chl) and thus the pertinent ratio is $R(510)/R(560)$. The results (Fig. 16b) demonstrate that the $r$-ratios extracted from the reflectance spectra follow rather well the semi-analytical algorithm, with a random dispersion of the points which is not wider than that observed for waters with low to moderate (Chl). There is no particular grouping when Groups 1 and 2 are considered separately nor a particular trend for the Bencal waters compared to waters of other oceanic zones with various trophic levels. Because the reflectance at 510 nm is weakly affected by the presence of yellow substance (at least in moderate concentration), the $R(510)/R(560)$ ratio can also cope with the Case 2-Y waters and provide (Chl). This conclusion probably would not hold true in case of higher yellow substance concentration.

The efficiency of the algorithm, based on the $R(510)/R(560)$ ratio and adapted for this high (Chl) range, declines when (Chl) increases. Indeed, with

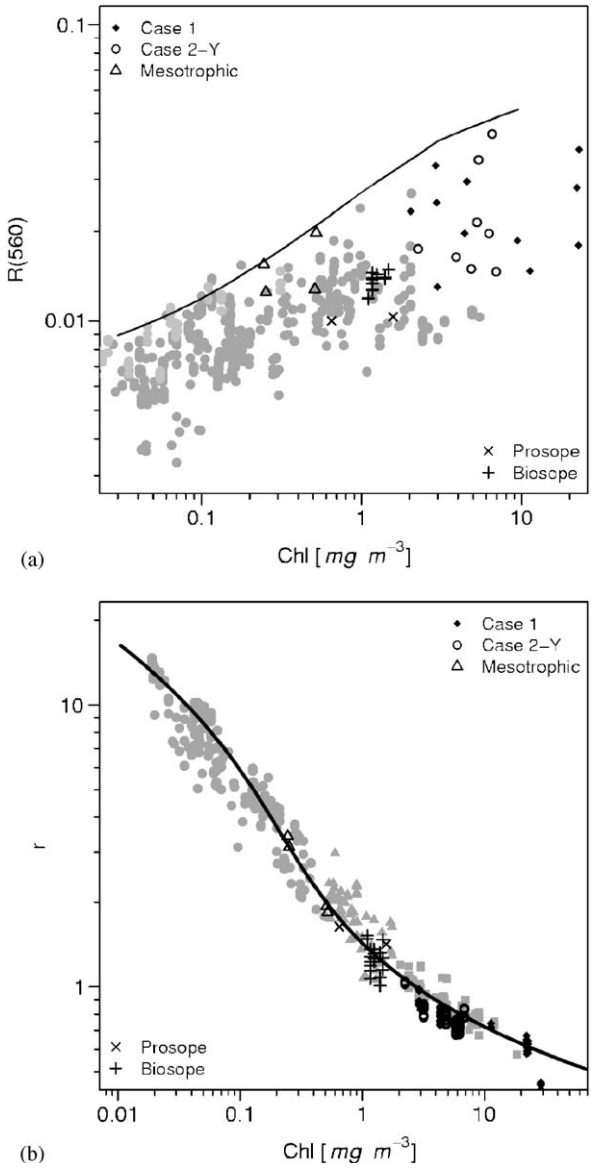


Figs. 16. (a) Reflectance values at 560 nm for Case 1 waters. The Bencal stations are specifically identified (diamonds and circles, as in Figs. 2 and 3), and superimposed onto other data from various locations in the world ocean, already shown in Morel and Maritorena (2001). The solid curve represents an upper limit for reflectance in Case 1 waters (see text). Recent data in eutrophic waters of the Moroccan (×) and Chilean (+) upwelling areas, (Prosope 1999 and Biospe 2004 cruises, respectively) are also shown. (b) Ratios of reflectances as a function of the chlorophyll concentration. The curve represents the polynomial expression (used as algorithm for MERIS), namely

$$\log_{10}(\mathrm{Chl}) = 0.406567 - 3.63030r + 5.4457r^2 - 5.48061r^3 + 1.75312r^4,$$

where $r = \log_{10}\{\max[(R443/R(560), R(490)/R(560), R(510)/R(560)]\}$. To the Bencal data are added recent data in eutrophic waters of the Moroccan (×) and Chilean (+) upwelling areas (see above). The gray symbols are for the previous data already used in Morel and Maritorena (2001). Note that the switches between the 1st and 2nd ratio, and the 2nd and 3rd ratio, occur at (Chl) ≈ 0.54, and (Chl) ≈ 2.25 mg m$^{-3}$, respectively.

the flattening of the modeled curve (Fig. 16b), small deviations in the value of the ratio (natural variability or inaccuracy in the marine signal retrieval) translate into important variations in the (Chl) assessment. This is an unavoidable (physical) limitation of the method, which makes any high (Chl) detected in ocean color imagery always imprecisely quantified.

## 7. Summary and conclusion

It is beyond the scope of this paper to discuss in detail the bio-optical properties of the Case 2-Y waters which are presented mainly for comparison with the high-Chl Case 1 waters, which are the focus of attention; several points deserve examination, as stated below:

(i) Do the bio-optical properties differ from what can be inferred from previous field observations for (Chl) ranges well below those of the present study?
(ii) Is the bio-optical variability in such high (Chl) waters larger than that already noticed for mesotrophic or oligotrophic waters?
(iii) Subsequently, and as a complementary question: Is an extrapolation toward high (Chl) of available bio-optical models for Case 1 waters still reliable?

For the first point, and regarding the absorption properties, it must be noted (Fig. 4) that $a_p(\lambda)$ increases nonlinearly with (Chl) with the usual slope (i.e. exponent). Yet, the observed values are systematically close to the upper limit of the relationships given in Bricaud et al. (1998), despite the fact that the relative contribution of non-algal particles is very low. The increase of the scattering coefficient (and of SPM and POC, Fig. 2), with increasing (Chl), follows trends that were previously observed at moderate (Chl). Since the apparent optical property $K_{bio}(\lambda)$ merges the (dominant) effect of absorption, and (to a lesser extent) that of scattering, it also increases regularly for increasing (Chl). Indeed (Fig. 7), the empirical relationships established between $K_{bio}(\lambda)$ and (Chl), in the domain of low and moderate (Chl), continue to apply for higher concentration, as summarized by Fig. 8. As a conclusion, the answer to the first question is negative, and there is a continuum within the optical properties over the whole (Chl) range.

With respect to the second question, it must be recalled that the natural variability affecting the previous empirical relationships between optical properties and (Chl) was high. Roughly speaking, for a given (Chl) value, coefficients like $a_p$, $b_p$, and $K_{bio}$ cannot be predicted from these relationships with an accuracy better than that corresponding to "within a factor 3" around the mean statistical value. The high-Chl waters are not exceptional from this viewpoint. The scatter of the $a_p$, $K_{bio}$, $b_p$, and SPM data (Figs. 4, 7, and 2) does not exceed this factor 3 within Group 1. Therefore, the bio-optical variability in these eutrophic waters is not significantly increased compared to that of mesotrophic waters. Admittedly, a sound answer to this second question would require that a more diversified dataset, including data from other upwelling zones, be analyzed.

To a certain extent, however, the measured bio-optical properties do not coincide closely with the modeled properties or the assumptions used in models (third question). Absorption and scattering properties will be successively examined. It appears (Fig. 11c) that the presently derived ($a_{tot} - a_w = a_p + a_y$) values are below those resulting from the model (Morel, 1988; Morel and Maritorena, 2001), particularly in the blue part of the spectrum. In this model, the terms $a_p$ and $a_y$ are not explicitly separated; on the contrary, they are merged as a result of an inversion of $K_d$. This model was developed for low to moderate (Chl), and if the $[a_y/(a_p + a_y)]$ ratio is on average larger in oligotrophic and mesotrophic waters than it is in eutrophic waters (see also Barnard et al., 1998), the model will lead to the observed overestimation at high (Chl). In the Gordon et al. (1988) radiance model, which makes a direct use of $K_d$, the situation is identical (but a fluctuating yellow substance component can be added). In other models (e.g. Sathyendranath and Platt, 1997), the $a_y$ term is systematically made proportional to the total particulate absorption at 440 nm, which likely is inappropriate, especially at high (Chl).

The scattering determinations show strongly featured spectra (Fig. 9a), with an absorption-induced minimum around 440 nm that deepens for increasing (Chl). This spectral behavior is well known from culture experiments (e.g. Ahn et al., 1992), but not regularly reported from field experiments; it was presently detected owing to the high phytoplankton concentration. It is generally not accounted for in semi-analytical bio-optical models

(but see Sathyendranath and Platt, 1997). In effect, $b_p$ is most often modeled as a monotonic power function of the wavelength ($\lambda^{-1}$ for instance, or a similar dependency), and $\tilde{b}_{bp}$ is generally assumed to be neutral, so that $b_{bp}$ and $b_p$ have the same spectral dependency. With such hypotheses, models cannot account for the observations in high-Chl waters. For the purpose of modeling $b_{bp}$, Gordon et al. (1988), see also (Gregg et al., 1993) placed the wavelength dependency and the depressive effect of absorption directly on $\tilde{b}_{bp}$, which is not supported by the results in Fig. 15. When the aim is only to model the reflectance, and thus to model $b_{bp}$ through the product ($b_p \times \tilde{b}_{bp}$), it is obviously equivalent to placing any $\lambda$-dependency, or any particular spectral feature, on $b_p$ or on $\tilde{b}_{bp}$. This is no longer legitimate when the purpose is to model optical properties other than the sole reflectance (e.g. radiance field or average cosines), for which the roles of $b_p$ and of $\tilde{b}_{bp}$ are distinct.

With regards to the magnitude of $\tilde{b}_{bp}$, the field values are above those predicted by various models, which points out a weakness. The modeled product $\tilde{b}_{bp}b_p$, however, accounts rather well for the measured $b_{bp}$ values at 550 nm (Fig. 15a), because the actual values of $b_p$ are generally lower than those predicted by the empirical Eq. (1′), and compensate for the increase in $\tilde{b}_{bp}$. More determinations of $\tilde{b}_{bp}$ in other high-Chl waters are needed to confirm the present values (around $10^{-2}$), which actually are not easily supported by theory. Indeed, for most phytoplankters, the backscattering ratio is below $10^{-3}$ (see e.g. Ahn et al., 1992). If it is believed that the phytoplankton-to-detritus ratio increases in high-Chl waters, then the $\tilde{b}_{bp}$ value would remain low. Admittedly, such a belief is based mainly on absorption properties and on carbon-to-Chl ratios (e.g. Loisel and Morel, 1998); it can be contested as far as the scattering and backscattering properties are concerned. Anyway, the understanding of the variability in the backscattering properties is still an open question (Stramski et al., 2004). The weakness of models (predicting "too low" $\tilde{b}_{bp}$ values) apparently has a limited impact on the modeled reflectance values, since the actual $R$-values are largely below the upper limit (curve in Fig. 17a), and the measured and modeled blue-to-green ratios (Fig. 17b) agree rather well, which is fortunate for remote sensing applications. In summary, the presently available models do not account accurately for the inherent optical properties ($a_y$, $b_p(\lambda)$, $\tilde{b}_{bp}$) observed in high Chl waters; the discrepancies, however, are not dramatic and are less marked when the apparent optical properties (as $K_d$ and $R$) are dealt with.

In reference to the initial questions in the Introduction, the optical variability of the algal cells themselves, which may occur in relation with the dominant species in eutrophic situations, is probably a second-order source of variability of the bulk optical properties. Finally, the main source originates from the looseness of the covariations between the detrital (dissolved and particulate) component and the algal stock, as already hinted at in Gordon and Morel (1983, pp. 65–67). There is growing evidence that in the open ocean, even in oligotrophic zones, the absorption by colored detrital (particulate and dissolved) organic materials (CDM) forms a notable and varying fraction of the total absorption (Bricaud et al., 1981; Siegel et al., 2002, 2005). In high-Chl Case 1 waters, this variability could even be higher, according to the age and the nutrient status of the algal population. The possibility of discriminating CDM and chlorophyll-bearing algae in satellite imagery is the subject of intense research (Lee et al., 2002; Maritorena et al., 2002; Siegel et al., 2005). Notwithstanding, the difficulties in effecting an accurate atmospheric correction in the near-UV, it is apparent that the extreme sensitivity of the reflectance at 370 nm to the CDM-to-living algae proportions is information that remains to be exploited.

## Acknowledgements

Funding of this program has been initially provided by the Marine and Coastal Management (MCM, Cape Town, South Africa), and supplemented by the National Aeronautics and Space Administration (NASA) and European Space Agency (ESA). These three Agencies are duly acknowledged. The captain, officers and crew of the research vessel *Africana* were all factors in the success of the campaign, as well as the expert guidance of Ray Barlow, Chief Scientist of the Bencal cruise. Stanford B. Hooker and James Aiken provided efficient help during field experiments. Preparation of the initial manuscript benefited from constructive discussions with Marcel Babin, Annick Bricaud, and Stewart Bernard, who also made available some unpublished data, and carefully processed the AC-9 data. We thank Patrick Raimbault who carried out the POC analyses. We

also thank two anonymous reviewers for their thorough reviews and helpful comments.

## References

Ahn, Y.-H., Bricaud, A., Morel, A., 1992. Light backscattering efficiency and related optical properties of some phytoplankters. Deep Sea Research 39, 1835–1855.

Austin, R.W., Petzold, T.J., 1986. Spectral dependence of the diffuse attenuation coefficient of light in ocean waters. Optical Engineering 25, 471–479.

Babin, M., Morel, A., Fournier-Sicre, V., Fell, F., Stramski, D., 2003. Light scattering properties of marine particles in coastal and open ocean waters as related to the particle mass concentration. Limnology and Oceanography 48, 843–859.

Baker, M., Smith, R.C., 1982. Bio-optical classification and model of natural waters. Limnology and Oceanography 27, 500–509.

Barlow, R., Sessions, H., Silulwane, N., Engel, H., Hooker, S.B., Aiken, J., Fishwick, J., Martinez-Vicente, V., Morel, A., Chami, M., Ras, J., Bernard, S., Pfaff, M., Brown, J.W., Fawcett, A., 2003. BENCAL cruise report. In: Hooker, S.B., Firestone, E.R. (Eds.), SeaWiFS Postlauch Technical Report Series. vol. 27, pp. 1–64.

Barnard, A.H., Pegau, W.S., Zaneveld, J.R.V., 1998. Global relationships of the inherent optical properties of the oceans. Journal of Geophysical Research 103, 24955–24968.

Bernard, S., Probyn, T.A., Barlow, R.G., 2001. Measured and modeled optical properties of particulate matter in the southern Benguela. South African Journal of Sciences 97, 410–420.

Boss, E., Pegau, W.S., Lee, M., Twardowski, M.S., Shybanov, E., Korotaev, G.B., Baratange, F., 2004. Particulate backscattering ratio at LEO 15 and its use to study particle composition and distribution. Journal of Geophysical Research 109, C01014.

Bricaud, A., Morel, A., 1986. Light attenuation and scattering by phytoplanktonic cells: a theoretical modeling. Applied Optics 25, 571–580.

Bricaud, A., Morel, A., 1987. Atmospheric corrections and interpretation of marine radiances in CZCS imagery: use of a reflectance model. Oceanologica Acta, SP, 33–50.

Bricaud, A., Stramski, D., 1990. Spectral absorption coefficients of living phytoplankton and nonalgal biogenous matter: a comparison between the Peru upwelling area and Sargasso Sea. Limnology and Oceanography 35, 562–582.

Bricaud, A., Morel, A., Prieur, L., 1981. Absorption by dissolved organic matter of the sea (yellow substance) in the UV and visible domains. Limnology and Oceanography 26, 43–53.

Bricaud, A., Babin, M., Morel, A., Claustre, H., 1995. Variability in the chlorophyll-specific absorption coefficients of natural phytoplankton: Analysis and parameterization. Journal of Geophysical Research 100, 13321–13332.

Bricaud, A., Morel, A., Babin, M., Allali, K., Claustre, H., 1998. Variations of light absorption by suspended particles with chlorophyll a concentration in oceanic (Case 1) waters: analysis and implications for bio-optical models. Journal of Geophysical Research 103, 31033–31044.

Bricaud, A., Claustre, H., Ras, J., Oubelkheir, K., 2004. Natural variability of phytoplanktonic absorption in oceanic waters: Influence of size structure of algal populations. Journal of Geophysical Research 109, C11010.

Clark, D.K., Baker, E.T., Strong, A.E., 1980. Upwelled spectral radiance distribution in relation to particulate matter in sea water. Boundary-layer Meteorology 18, 287–298.

Gordon, H.R., 1989. Can the Lambert-Beer law be applied to the diffuse attenuation coefficient of ocean water? Limnology and Oceanography 34, 1389–1409.

Gordon, H.R., 2002. Inverse methods in hydrologic optics. Oceanologia 44, 9–58.

Gordon, H.R., Morel, A., 1983. Remote assessment of ocean color for interpretation of satellite visible imagery: a review. Lecture Notes on Coastal and Estuarine Studies, vol. 4. Springer, New York, p. 114.

Gordon, H.R., Brown, O.B., Jacobs, M.M., 1975. Computed relations between inherent and apparent optical properties of a flat homogeneous ocean. Applied Optics 14, 417–427.

Gordon, H.R., Brown, O.B., Ewans, R.H., Brown, J.W., Smith, R.C., Baker, K.S., Clark, D.K., 1988. A semi-analytical radiance model of ocean color. Journal of Geophysical Research 93, 10909–10924.

Gower, J.F.R., Doerffer, R., Borstad, G.A., 1999. Interpretation of the 685 nm peak in water-leaving radiance in terms pf fluorescence, absorption, and scattering, and its observation by MERIS. International Journal of remote Sensing 20, 1771–1786.

Gregg, W.W., Chen, F.C., Mesaache, A.L., Chen, J.D., Whiting, J.F., 1993. The simulated SeaWiFS data set. In: Hooker, S.B. (Ed.), SeaWiFS Technical Report Series. NASATech. Memo, 1999-206892. vol. 9. pp. 1–17.

Hooker, S.B., Van Heukelem, L., Thomas, C.S., Claustre, H., Ras, J., Barlow, R., Sessions, H., Schluter, L., Perl, J., Trees, C., Stuart, V., Head, E., Clementson, L., Fishwick, J., Llewellyn, C., Aiken, J., 2005. The Second SeaWiFS HPLC Analysis Round-robin Experiment (SeaHARRE-2). NASA/TM-2005-212785, pp. 1–112.

Kishino, M., Takahashi, M., Okami, N., Ichimura, S., 1985. Estimation of the spectral absorption coefficients of phytoplankton in the sea. Bulletin of Marine Sciences 37, 634–642.

Lazzara, L., Bricaud, A., Claustre, H., 1996. Spectral absorption and fluorescence excitation properties of phytoplankton populations at a mesotrophic and an oligotrophic site in tropical North Atlantic (EUMELI Program). Deep Sea Research I 43, 1215–1240.

Lee, Z.P., Carder, K.L., Arnone, R., 2002. Deriving inherent optical properties from water color: a multiband quasi-analytical algorithm for optically deep waters. Applied Optics 27, 5755–5772.

Loisel, H., Morel, A., 1998. Light scattering and chlorophyll concentration in Case 1 waters: a reexamination. Limnology and Oceanography 43, 847–858.

Maritorena, S., Siegel, D.A., Peterson, A., 2002. Optimization of a semi-analytical ocean color model for global applications. Applied Optics 41, 2705–2714.

Morel, A., 1988. Optical modeling of the upper ocean in relation to its biogenous matter content. Journal of Geophysical Research 93, 10749–10768.

Morel, A., Belanger, S., 2006. Improved detection of turbid waters from ocean color sensors information. Remote Sensing of Environment 102, 237–249.

Morel, A., Gentili, B., 2004. Radiation transport within oceanic (Case 1) water. Journal of Geophysical Research 109.

Morel, A., Maritorena, S., 2001. Bio-optical properties of oceanic waters: a reappraisal. Journal of Geophysical Research 106, 7163–7180.

Morel, A., Antoine, D., Gentili, B., 2002. Bidirectional reflectance of oceanic waters: accounting for Raman emission and varying particle scattering phase function. Applied Optics 41, 6289–6306.

O'Reilly, J.E., Maritorena, S., Mitchell, B.G., Siegel, D.A., Carder, K.L., Garver, S.A., Kahru, M., McClain, C., 1998. Ocean color algorithms for SeaWiFS. Journal of Geophysical Research 103, 24937–24953.

Sathyendranath, S., Cota, G., Stuart, V., Maas, H., Platt, T., 2001. Remote sensing of phytoplankton pigments: a comparison of empirical and theoretical approaches. International Journal of remote Sensing 22, 249–273.

Sathyendranath, S., Platt, T., 1997. Analytic model of ocean color. Applied Optics 36, 2620–2629.

Siegel, D.A., Maritorena, S., Nelson, N.B., Hansell, D.A., Lorenzi-Kayser, M., 2002. Global ocean distribution and dynamics of colored dissolved and detrital organic material. Journal of Geophysical Research 107 (C12), 3328.

Siegel, D.A., Maritorena, S., Nelson, N.B., Behrenfeld, M.J., 2005. Independence and interdependencies of global ocean color properties: re-assessing the bio-optical assumption. Journal of Geophysical Research 110 (C07011).

Staehr, P.A., Markager, S., 2004. Parameterization of the chlorophyll a specific in vivo light absorption coefficient covering estuarine, coastal, and oceanic waters. International Journal of Remote Sensing 25, 5117–5130.

Stramska, M., Stramski, D., Hapter, R., Kaczmarek, S., Ston, J., 2003. Bio-optical relationships and ocean color algorithms for the north polar region of the Atlantic. Journal of Geophysical Research 108 (C5), 3143.

Stramski, D., Boss, E., Bogucki, D., Voss, K.J., 2004. The role of seawater constituents in light backscattering in the ocean. Progress in Oceanography 61, 27–56.

Sullivan, J.M., Twardowski, M.S., Donaghay, P.L., Freeman, S.A., 2005. Use of optical scattering to discriminate particle types in coastal waters. Applied Optics 44, 1667–1680.

Twardowski, M.S., Boss, E., Macdonald, J.B., Pegau, W.S., Barnard, A., Zaneveld, J.R.V., 2001. A model for estimating bulk refractive index from the optical backscattering ratio and the implications for understanding particle composition in case I and case II waters. Journal of Geophysical Research 106, 14129–14142.

Ulloa, O., Sathyendranath, S., Platt, T., 1994. Effect of particle-size distribution on the backscattering ratio in seawater. Applied Optics 33, 7070–7077.

Vidussi, F., Claustre, H., Manca, B.B., Luchetta, A., Marty, J.C., 2001. Phytoplankton pigment distribution in relation to upper thermocline circulation in the eastern Mediterranean Sea during winter. Journal of Geophysical Research 106, 19939–19956.

Werdell, P.J., Bailey, S.W., 2005. An improved in-situ bio-optical dataset for ocean color algorithm development and satellite data product validation. Remote Sensing of Environment 98, 122–140.